Journal of Biomedical Optics

SPIEDigitalLibrary.org/jbo

Eumelanin fibrils

Ross McQueenie
Jens Sutter
Jan Karolin
David J. S. Birch

SPIE

Eumelanin fibrils

Ross McQueenie, Jens Sutter, Jan Karolin, and David J. S. Birch
University of Strathclyde, Department of Physics, Photophysics Group, Centre for Molecular Nanometrology, SUPA, Glasgow, G4 0NG, Scotland

Abstract. We describe the auto-oxidation of 3, 4-dihydroxy-L-phenylalanine (L-DOPA) in the synthesis of eumelanin to spontaneously produce fibrils upon drying. The self-assembled fibrils are of characteristic diameter ~1 to 2 μm, composed of filaments, and are unidirectional, apart from branches that are formed at typically an angle of 20 to 22 deg. The fibrils are characterized using fluorescence spectroscopy, fluorescence decay times, scanning electron microscopy, atomic force microscopy, and fluorescence lifetime imaging microscopy. The fibrils mimic natural melanin in consisting of core eumelanin with efficient nonradiative properties, but they also display pockets of electronically isolated species with higher radiative rates on the nanosecond timescale. Eumelanin fibrils formed occasionally in solution are tentatively attributed to a scaffold of bacteria or fungus. Fabricating and characterizing novel synthetic eumelanin structures such as fibrils are of interest in helping to reveal a functional structure for eumelanin, in understanding its photophysics, in learning more about L-DOPA as it is used in the treatment of Parkinson's disease, and in producing novel materials which might embody some of the diverse properties of eumelanin. [DOI: 10.1117/1.JBO.17.7.075001]

Keywords: eumelanin; fibril; 3, 4-dihydroxy-L-phenylalanine; fluorescence lifetime imaging microscopy.

Paper 12074 received Feb. 7, 2012; revised manuscript received May 2, 2012; accepted for publication May 17, 2012; published online Jul. 9, 2012.

1 Introduction

Melanins are ubiquitous pigments in plants, animals, and humans. Of the two types present in humans, brown-black eumelanin and yellow-red pheomelanin, eumelanin is the most common and imparts color to human skin, hair, and eyes. Although not fully substantiated, the most widely accepted model for eumelanin is that of a nonrepeating biopolymer of aggregated π–stacked planar and cross-linked heterogeneous structures of indolequinone monomers.[1] Studies on *Sepia officinalis*, a natural eumelanin extracted from the ink sac of cuttlefish, confirm native eumelanin morphology to be a nanoparticle of diameter ~150 nm,[2] with the fundamental unit of ~10 nm diameter.[3] In this paper we describe the fabrication and characterization of a more expansive eumelanin morphology, namely dendrite-like fibrils of diameter of ~2 to 3 μm that are formed on a mm scale, after self-assembly upon drying during the nonenzymatic oxidation of a key component in human eumelanogenesis, 3,4-dihydroxy-L-phenylalanine (L-DOPA). The drying of eumelanin is of interest as it may potentially reproduce some of the characteristics of the assembly and morphology of natural melanin. These are not only of biochemical interest, but also with regard to the development of new materials that might make use of eumelanin's properties, such as photoconductivity and metal ion binding. Eumelanin fibrillation, which seems to have been little studied, has bearing on our general understanding of fibril formation, as well as possibly the neurological diseases Alzheimer's,[4] Huntington's,[5] and Parkinson's.[6] This is because L-DOPA forms the basis of a therapeutic for the latter since it readily crosses the blood-brain barrier to release dopamine. Recent AFM studies have revealed morphological details on L-DOPA-eumelanin fibrils of width ~250 nm and depth ~50 nm that are formed upon drying shortly after aeration.[7] Here we present results on the spectroscopy and microscopy of L-DOPA-eumelanin fibrils and discuss them in the context of more commonly studied morphologies for eumelanin.

Fibrillation is a generic occurrence in material science that encompasses multifarious materials and mechanisms of self-assembly. For example, glucose forming cellulose, diamine and carboxylic acid forming nylon, polypeptide aggregation to form collagen, and protein aggregation. The latter has received global attention in recent times in the drive to understand the molecular mechanisms responsible for a number of neurodegenerative diseases. By way of contrast melanin has to date been investigated largely in terms of a bio-nanoparticle rather than from the standpoint of spontaneous fibril formation.

Indeed, the Raper-Mason pathway[8] (summarized in Fig. 1), which is often used to describe melanogenesis in vertebrates, requires the enzyme tyrosinase to catalyze the oxidation of tyrosine and L-DOPA to form dopaquinone, which rapidly undergoes internal cyclization to form dopachrome and subsequently 5,6-dihydroxyindole (DHI) and 5,6-dihydroxyindole-2-carboxylic acid (DHICA). The oxidation of these primary structures, either spontaneously or catalyzed, is then thought to give rise to oligomers composed of 4 to 5 indolequinone monomers, which x-ray diffraction studies have shown then aggregate into π–stacked planar and cross-linked structures[1] to form nanoparticles. Despite a lack of knowledge as to how these monomers are actually connected together, this model of native eumelanin as an enzyme-facilitated bio-nanoparticle has been researched extensively and become well-established. By association this nanoparticle description might be thought to simply translate to the structure of nonenzymatic melanin synthesized from L-DOPA. Moreover, despite extensive spectroscopic studies of both natural and synthetic melanin, microscopic studies to date have by and large been confined to the former. Here we

Address all correspondence to: David J. S. Birch, University of Strathclyde, Department of Physics, Photophysics Group, Centre for Molecular Nanometrology, SUPA, Glasgow, G4 0NG, Scotland. Tel: 441 41 548 3377; Fax: 441 41 552 2891; E-mail: djs.birch@strath.ac.uk.

0091-3286/2012/$25.00 © 2012 SPIE

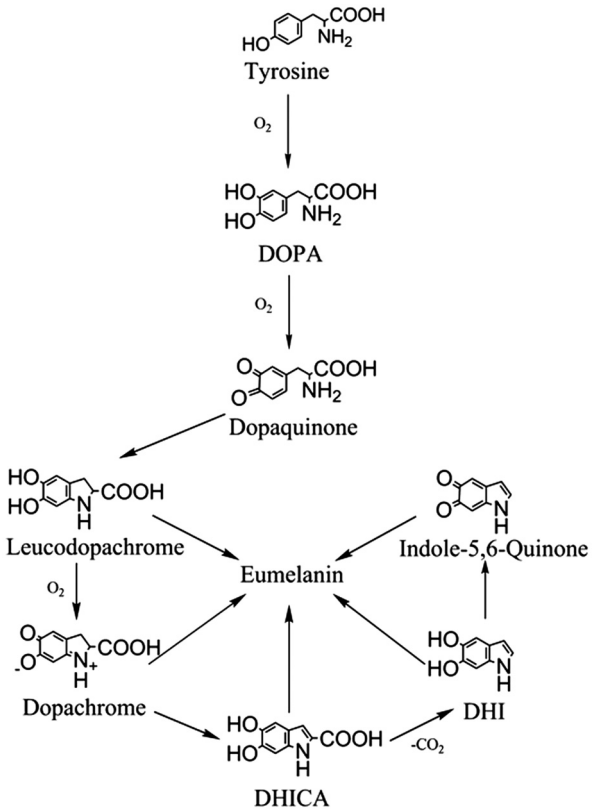

Fig. 1 The eumelanin synthetic pathway.[8] Melanogenesis requires the enzyme tyrosinase to catalyze the oxidation of tyrosine and L-DOPA. *In vitro* auto-oxidation occurs readily and increases with pH, temperature and aeration to produce synthetic eumelanin formed from a complex mixture of reaction products as illustrated.

describe how the structural product from the laboratory oxidative synthesis of eumelanin from L-DOPA can, under certain conditions, be fibril in nature rather than particulate, and displays similar spectroscopic properties to naturally occurring melanin. The fibrils can grow to the mm scale and we have characterized them using microscopy with atomic force microscopy (AFM), scanning electron microscopy (SEM), and fluorescence lifetime imaging microscopy (FLIM) as well as absorption spectroscopy and intrinsic fluorescence spectroscopy.

The use of intrinsic (as against extrinsic) fluorophores as a probe has clear advantages in terms of preserving native structures by perturbing them less and being more sensitive to their change. In the context of fibrils this has been demonstrated recently by the use of changes in tyrosine conformation to monitor β-amyloid fibril formation associated with Alzheimer's disease at the early oligomer stages rather than using extrinsic probes such as Thioflavin T and Congo red, which only detect the β-sheets that are formed much later.[9] Here we are able to make use of the intrinsic fluorescence of synthetic eumelanin in imaging by using photon counting detection and multiphoton excitation, even though the fluorescence quantum yield can be extremely low under certain conditions ($<7 \times 10^{-4}$ for UV excitation).[10]

2 Experimental Details

L-DOPA was dissolved from powdered form at a concentration of 1 mM in de-ionized water, which was free of background fluorescence. The rate of eumelanin formation is much slower at pH 7 than pH 10, but increases with temperature and saturation with oxygen. Hence air was bubbled through each sample for 48 h at a flow rate of 1.5 L/ min in order to saturate with oxygen ($[O_2] \sim 1$ mM), at 37°C in the case of pH 7, and room temperature in the case of pH 10. Ammonia was added at 0.17 mM in order to obtain pH 10 when required. Ammonia was used in place of conventional bases used for eumelanin oxidation such as sodium hydroxide and borate buffer. When depositing sodium hydroxide onto microscope slides, crystallization was observed and therefore microscopy was not possible, whilst borate is known to complex with L-DOPA, which may affect the synthetic pathway. The formation of eumelanin was suggested by observing the color in the sample change from clear solution to a dark red after approximately 4 h, then to an inky-black after 48 h. The sample was then incubated in the dark for a period of two weeks at room temperature. After this period the fibrils were formed upon drying on glass slides which were cleaned of contaminants using a dilute mixture of 5% potassium hydroxide in methanol and treated to be hydrophilic using a dilute mixture of water, ammonium hydroxide, and hydrogen peroxide in a 5 : 1 : 1 ratio. All chemicals were purchased in purest form from Sigma Aldrich.

Fluorescence lifetime imaging microscopy (FLIM) was performed using a Zeiss LSM 510 laser-scanning microscope recorded through a 10× objective water-immersion lens. Excitation of samples on the microscope slide was via a Coherent Chameleon wavelength-tunable laser set at wavelengths of either 800 or 900 nm to induce two-photon excitation. The maximum power of the laser is 2.5 W at 800 nm and 1.7 W at 900 nm. Fluorescence from both excitation wavelengths was recorded over the same area of a single sample, and collected over the spectral region 435 to 485 nm. The FLIM time resolution, as defined by the shortest measureable decay time, is ~200 ps. Optical images were taken by a Nikon D300 camera modified to fit on the external viewing port of the FLIM system by use of a T-2 Nikon bayonet adapter. AFM images are taken on a Witec Alpha SNOM with AFM adaptor in which is a 285 kHz resonance tip for high-resolution images. SEM images are taken on an FEI Sirion 200 field emission scanning electron microscope. Fluorescence decay time measurements in bulk solution were obtained in 1 cm path-length quartz cuvettes at a L-DOPA concentration of 40 μM using a Horiba Jobin IBH FluoroCube incorporating time-correlated single-photon counting (TCSPC) and NanoLED[11] excitation at 375 nm, with the emission being collected at 480 nm. The time resolution is better than the 200 ps for FLIM and nearer to 100 ps for multi-exponential analysis of TCSPC data. A χ^2 fitting parameter and weighted residuals were used to evaluate the goodness of fit of the measured decay to an exponential function

$$I(t) = \sum_{i=1}^{n} \alpha_i \exp\left(-\frac{t}{\tau_i}\right), \tag{1}$$

where α_i is a pre-exponential factor determining the contribution of each decay time component to the overall decay and τ_i is a fluorescence decay time. For the FLIM data $n = 2$ was found to be sufficient, though for the higher statistical precision of TCSPC data $n = 3$ was required to give a good fit to the data. For comparison we also performed a model-free analysis of the TCSPC data based on maximum entropy in order to obtain a decay time distribution function in the manner we used previously when studying β-amyloid aggregation.[9]

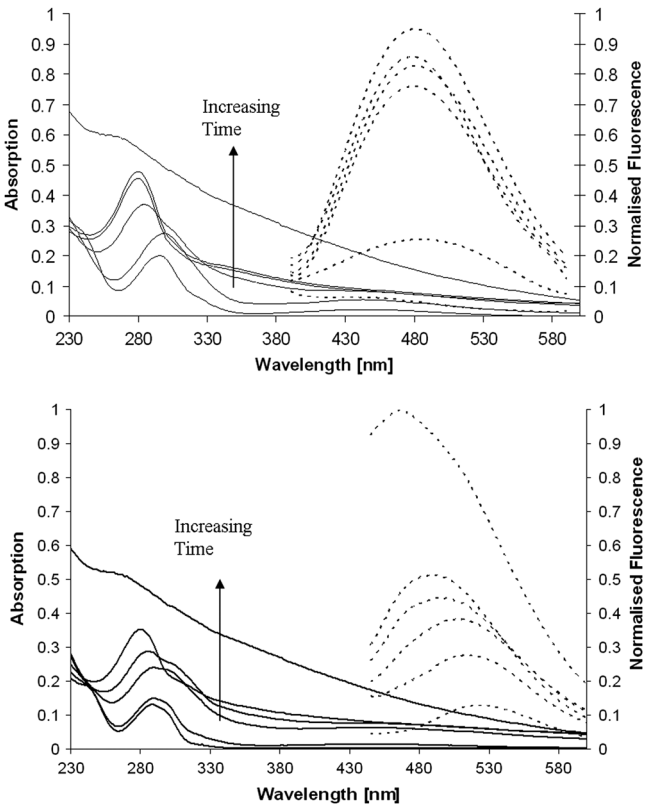

Fig. 2 Steady-state absorption (solid line) and fluorescence (dashed line) spectra excited at 375 nm of 40 μM L-DOPA in water. (a) pH 7 at 37°C and bubbled with air to saturate with oxygen (~1 mM) showing production of eumelanin from L-DOPA. The times are 0.5, 1, 2, 5, 24, and 48 h. (b) pH 10 and bubbled with air to saturation at room temperature. The times are 0.5, 1, 4, 6, 25, and 48 h.

3 Results and Discussion

Absorption and fluorescence spectral measurements were obtained during the first 48 h of eumelanin formation as shown in Fig. 2. Although the scheme shown in Fig. 1 is inherently complex, with overlapping and transient structures, and not fully understood, some likely components are identifiable from their spectroscopy. In addition to color changes, the formation of eumelanin was suggested from the gradual broadening of the steady-state absorption spectrum, the loss of the characteristic L-DOPA absorption spectral peak around 280 to 300 nm, the emergence of the characteristic dopachrome absorption at ~400 to 500 nm,[12] and the gradual increase in fluorescence when excited at 375 nm. Recent work has suggested the latter corresponds to excitation of a major end-product, dihydroxyindole-carboxylic acid (DHICA).[13] The constancy of the fluorescence spectral peak at ~480 nm at pH 7 suggests the core oligomeric species, including DHICA, are formed early in the polymerization and remain little changed. At later times little fluorescence is observed when exciting the L-DOPA monomer band at ≤330 nm. These trends are consistent with what is known for eumelanin formation and monomers such as DHI, DHICA, and their indolequinones, which are π and/or hydrogen bonded. By contrast the fluorescence spectra at pH 10 show a blue peak shift during polymerization suggesting the less stable structures formed early in the polymerization, including dopachrome, proceed more slowly due to deprotonation towards the more stable end product of DHICA. This overall constancy in the photophysical structures during polymerization at pH 7 is borne out by the fluorescence decay time data obtained using TCSPC where two decay components remain steady at ~0.2 ns and ~1.2 to 1.4 ns while a third component decreases from ~8 to 6 ns over 350 h (see Table 1). Decay times at pH 10 shown in Table 2 differ in that more systematic changes occur in two not one of the decay components. At both pH 7 and pH 10 the effectively same decay components at 48 and 350 h suggest the final structures are already in place within 48 h. The decay components we record are consistent with the three components reported previously for two-photon excitation of synthetic eumelanin in dimethyl sulphoxide.[14] However, although Tables 1 and 2 demonstrate that three exponentials provide a good description of the data, and are sufficient to reveal the major trends, a maximum entropy analysis revealed evidence for the emergence after ~6 h of a fourth decay component. Previously we reported four decay components for *S. officinalis* that were particle size-dependent.[15] Here the dominant ~6 ns component in Tables 1 and 2 is seen to split into a shorter and longer component at later times when using maximum entropy analysis, with the two faster components of the three exponential analysis of ~0.2 ns

Table 1 Fluorescence decay time values at pH 7 for eumelanin forming from 40 μM L-DOPA solution. Initially there was 48 h of aeration at 37°C with data recorded between 0.5 and 350 h. Fluorescence lifetime decays are fitted to three-exponentials, with the χ^2 value indicating it is an appropriate fitting regime (<1.2). Samples were excited at 375 nm and emission collected at 480 nm using TCSPC. Errors shown are 3 standard deviations.

Time/hr	τ_1/ns	α_1/%	τ_2/ns	α_2/%	τ_3/ns	α_3/%	χ^2
0.5	1.19 ± 0.10	33	8.32 ± 0.20	44	0.24 ± 0.10	23	1.16
1	1.26 ± 0.12	34	9.32 ± 0.15	47	0.25 ± 0.10	19	1.17
3	1.45 ± 0.12	37	8.47 ± 0.15	43	0.21 ± 0.10	20	1.16
5	1.44 ± 0.11	32	8.74 ± 0.17	46	0.20 ± 0.10	22	1.18
24	1.37 ± 0.18	19	6.49 ± 0.15	55	0.19 ± 0.10	26	1.20
26	1.28 ± 0.10	21	6.40 ± 0.14	55	0.19 ± 0.10	24	1.20
48	1.20 ± 0.19	20	6.27 ± 0.18	54	0.18 ± 0.10	26	1.18
350	1.18 ± 0.19	21	6.19 ± 0.19	53	0.18 ± 0.10	26	1.18

Table 2 Fluorescence decay time values of eumelanin forming from L-DOPA solution as a function of polymerization time at room temperature and pH 10 including an initial 48 h of aeration. Samples were excited at 375 nm and emission was collected at 480 nm using TCSPC. Errors shown are 3 standard deviations.

Time/hr	τ_1/ns	α_1/%	τ_2/ns	α_2/%	τ_3/ns	α_3/%	χ^2
0.5	1.49 ± 0.10	22	7.94 ± 0.09	67	0.22 ± 0.10	11	1.19
1	1.41 ± 0.07	38	7.06 ± 0.16	40	0.14 ± 0.10	22	1.19
4	1.39 ± 0.08	40	5.93 ± 0.20	29	0.17 ± 0.10	31	1.11
6	1.31 ± 0.10	38	4.79 ± 0.17	30	0.18 ± 0.10	32	1.17
25	1.22 ± 0.10	33	4.81 ± 0.11	45	0.13 ± 0.10	22	1.19
48	1.74 ± 0.10	38	6.63 ± 0.16	42	0.19 ± 0.10	20	1.19
336	1.78 ± 0.10	39	6.80 ± 0.16	46	0.19 ± 0.10	15	1.18

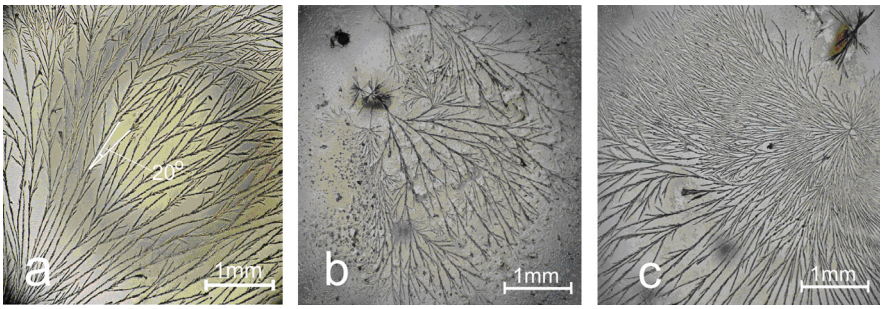

Fig. 3 Typical two week old L-DOPA fibrils at pH 10 observed by bright field microscopy.

and ~1.2 to 1.8 ns being largely preserved. It would be tempting to try and associate the number of decay components to the number of excited states and thereby species present. However, given the complex nature of eumelanin this would be likely to be somewhat speculative.

Figure 3 shows bright field microscopy images for L-DOPA solution dried on a glass slide. Dendrite-like fibril structures are clearly evident with branching observed throughout the sample, which is predominantly at an angle of 20 to 22 deg to the core strand. The lack of entanglement of these dried structures suggests they do not pre-exist in solution, but are formed by deposition during the drying. We thus investigated these structures further using FLIM.

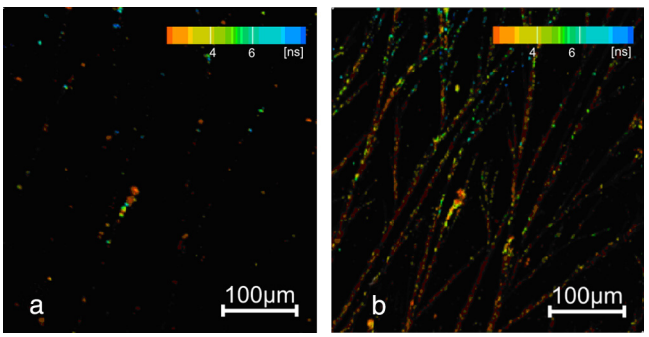

Fig. 4 Fluorescence lifetime images of eumelanin fibrils formed at pH 10 with excitation wavelengths (a) 800 nm and (b) 900 nm. Color scale indicates the longer fluorescence decay time components over the range of 2 to 8 ns (see Table 3).

Figure 4(a) and 4(b) shows multiphoton FLIM images of decay time components in the range ~2 to 8 ns when excited at (a) 800 nm and (b) 900 nm after two weeks of L-DOPA solution incubation at pH 10. Figure 5(a) and 5(b) shows the shorter decay time components in the range ~100 to 500 ps, with most of the emission found to be <200 ps. Each scan at both excitation wavelengths is taken over the same area of the sample of dimensions $420 \times 420\ \mu m^2$. The quenched fluorescence from most of the fibril core is consistent with the efficient nonradiative processes in eumelanin.[10,16]

The two-photon FLIM of decay time components formed at pH 10, and also pH 7 (not shown) after drying show evidence of a heterogeneous distribution of photophysical species. Although two-photon excited fluorescence spectra and decay times of synthetic eumelanin have been reported,[14] to the best of our knowledge these figures represent the first two-photon fluorescence images of a eumelanin structure. Analysis of the two-photon images reveal bi-exponential fluorescence decay components of 2 to 3 ns and 100 to 200 ps throughout the fibrils (Table 3). Although undoubtedly an approximation, the bi-exponential fluorescence temporal decay function used to analyze the FLIM data is found to be sufficient to reveal the dominant trends and features. Under closer inspection the fibrils are shown to be composed of mainly ≤200 ps decay time with pockets of the longer decay times embedded within them. It seems likely these local pockets of longer decay times can be attributed to

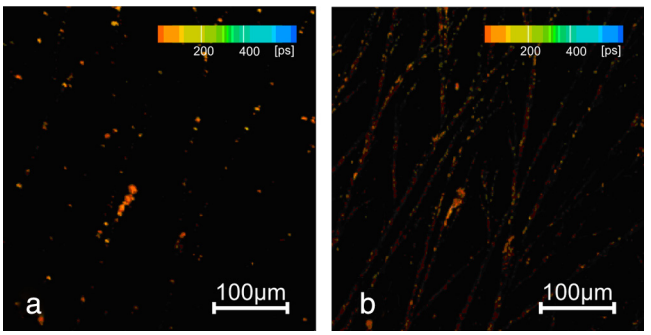

Fig. 5 Fluorescence lifetime images of eumelanin fibrils formed at pH 10 with excitation wavelengths (a) 800 nm and (b) 900 nm. Color scale indicates the shorter fluorescence decay components in the range of up to 200 ps (see Table 3). Note the same color scale is used to denote the different time ranges of Figs. 4 and 5.

Table 3 Bi-exponential fit to the dried fibril fluorescence decay using two-photon excitation at 800 and 900 nm. Values were obtained from single pixels on FLIM images.

Excitation/nm	τ_1/ns	α_1/%	τ_2/ns	α_2/%	χ^2
800	≤0.2	83.2	2.6	16.8	1.17
900	≤0.2	87.6	3.3	12.4	1.18

electronically isolated and self-aggregated indolic monomer/oligomeric structures formed from dopachrome or DHICA[10] on the outer regions of the fibril, which bind to the fibril later in the assembly process, are not fully polymerized into the core structure and hence not quenched by being in close proximity to other structures.[16] Certainly more intense fluorescence is observed from the 900 nm excitation as compared to that at 800 nm despite the 30% less laser power at 900 nm. The possibility of hyper-Rayleigh scattering anomalously accounting for this was investigated spectrally and ruled out giving credence to there being higher absorption at 900 nm. This would be consistent with the presence of extended π electron structures such as the stacking of oligomer planes or electronically isolated oxidation products such as dopachrome and DHICA. Indeed the one-photon equivalent of 900 nm two-photon excitation is the 450 nm excitation leading to 480 nm fluorescence that is consistent with the identification of the dopachrome band in Fig. 2.[12] This perhaps contrasts with previous ultrafast spectroscopic studies of synthetic eumelanin in dimethyl sulfoxide, where the possibility of the two photon excitation at 800 nm being via a stepwise resonant real intermediate state[14] rather than via a virtual state as would be required to stimulate dopachrome and DHICA fluorescence was muted.

Taken together, the results so far suggest a complex heterogeneous structure to the fibrils based on fundamental oligomer units with unique photophysics, which are formed early in the growth process, endure, and remain distinct even on drying.

AFM images (Fig. 6) show the fibrils at the microscopic scale, between 5×5 μm and 50×50 μm. These high-resolution images reveal the fibrils are typically 1 to 2 μm in diameter with branching and some evidence of being formed from thinner filaments bundled together though less intertwined than protofibrils in amyloids.[17] These features are further demonstrated by SEM images as shown in Fig. 7. The branching is clear in the SEM images but the cracking observed upon drying means the evidence for the joining of smaller filaments is not as compelling as the AFM images. For both the AFM and SEM images no structures are visible on the external surfaces that might correlate with the fluorescent pockets observed in the FLIM measurements. Although the optical microscope images might suggest fractal behavior, the AFM and SEM images clearly show the structures are not fractal. Previously, smaller filaments of ~250 nm width have been reported using AFM, but these were obtained immediately after 72 h aeration[7] and not the 48 h aeration and two weeks incubation we have employed. Hence it seems possible the longer incubation time we are working with allows smaller filaments time to combine to produce the larger fibrils that we observe; although we cannot rule out we are simply observing the aggregation of larger structures. Similar dendrite-like structures to what we observe, not granule formation, have also been previously observed when drying natural melanin from *S. officinalis*,[3] suggesting the process of granule formation in natural melanin is not easily reproduced *in vitro*.

Common features of all the microscope images presented are the 20 to 22 deg branching angle in the forward direction, the unidirectional nature of the spines and branches and lack of entanglement, in marked contrast to many other related protein/peptide fibrils which do not branch, for example β-amyloid,[18] although branching at a typical angle of 35 to 40 deg has recently been reported in fibrils formed from the peptide hormone glycagon.[19] The origin of the branching is unclear, but the FLIM evidence suggests it is does not occur at the pockets of longer decay times. It may originate with the untwining of a filament or alternatively during the growing of a filament through binding to the like of hydroxyl, carboxylic acid, and amine groups that are present. Like eumelanin's native bionanoparticle form, questions arise as to how synthetic eumelanin

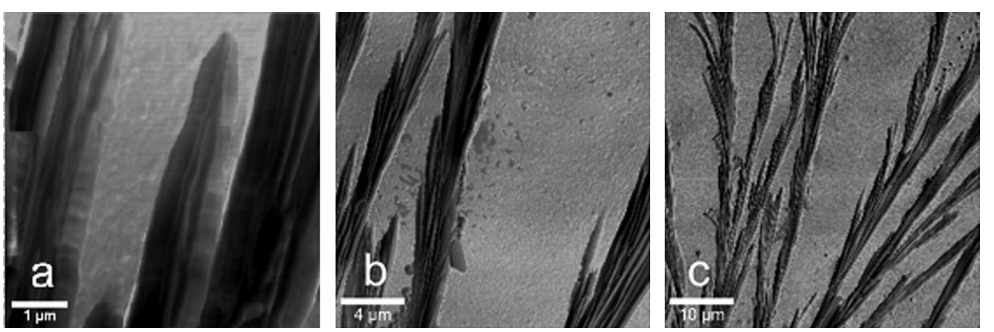

Fig. 6 Atomic force microscopy phase images of pH 10 eumelanin fibrils of resolution (a) 5×5 μm, (b) 20×20 μm, and (c) 50×50 μm.

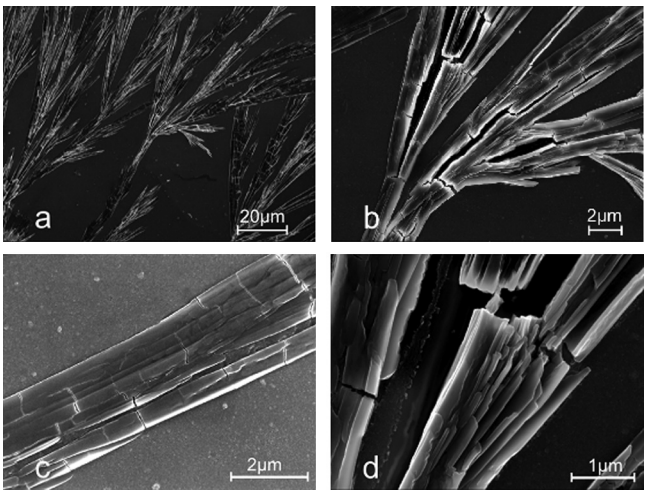

Fig. 7 Scanning electron microscopy images of pH 10 eumelanin fibrils at (a) 1000× magnification, (b) 6500× magnification, (c) 15000× magnification, and (d) 25000× magnification.

Table 4 Bi-exponential fit to the fluorescence decay of wet fibrils after six weeks incubation according to the data and conditions of Fig. 8 using two-photon excitation at 900 nm (800 nm excitation data also shown). Values were obtained from single pixels on FLIM images.

Excitation/nm	τ_1/ns	α_1/%	τ_2/ns	α_2/%	χ^2
800	≤0.2	80.5	1.6	19.5	1.16
900	≤0.2	84.1	2.8	15.9	1.16

fibrils assemble, what their secondary structure is, and how eumelanin's molecular structure in particle and fibril forms might differ.

Although the fibrils discussed so far have been formed on drying eumelanin we have also investigated the possibility of L-DOPA forming eumelanin fibrils in solution. Despite extensive investigation under neutral and alkaline conditions, we find this does not happen readily or reproducibly, but can happen occasionally. Figure 8 shows such an example of an aqueous solution FLIM measurement at pH 7 bearing many of the hallmarks of the dried eumelanin shown in Figs. 4 and 5. Again, dominant decay components of ≤ 200 ps are complemented by less abundant and longer decay components in the nanosecond region as shown in Table 4. The wet fibrils show evidence of a more continuous distribution of these longer and faster decay components rather than pockets of longer decay time amongst the more abundant and quenched bulk core of the dried fibrils. The tangling of the fibrils is in contrast to Figs. 4 and 5 and indeed suggests they are pre-formed in solution and not upon drying. We tentatively attribute this occasional formation of fibrils in solution to the influence of a fungal (or bacterial) synthetic pathway for eumelanin polymerization providing a scaffold for fibril growth over a long time, in our case some six weeks.[20]

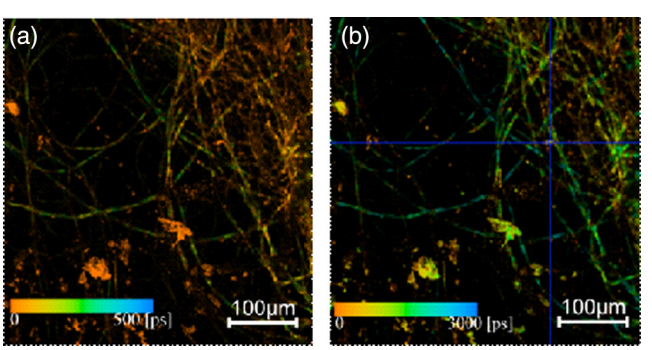

Fig. 8 FLIM image of L-DOPA fibrils formed after six weeks at room temperature incubation of 1 mM DOPA in distilled water at pH 7 after initial 48 h of aeration at 37°C. FLIM images show lifetime distributions by color for the (a) τ_1 and (b) τ_2 components after excitation at 900 nm. This data shows dominant decay components of typically $\tau_1 \sim 100$ to 200 ps and $\tau_2 \sim 2$ ns of relative abundance ~80% and 20%, respectively. Note the same color scale is used to denote the different time ranges of each image.

4 Conclusions

Despite global attention, over decades of research, melanin remains one of the most enigmatic of pigments. It is known to play a key role in photo-protection and malignant melanoma[21] and yet its kinetics of self-assembly, and secondary structure that define the minimum functional unit (protomolecule), remain unresolved. Its optical spectroscopy is complex and even its broad-band absorption spectrum is open to different explanations. It exists in the brain and we do not know what its neurological purpose is although significant correlations have been noted. For example, the loss of neuromelanin has been directly linked to Parkinson's disease[22] and the latter to melanoma.[23] The contrast between melanin's importance and lack of understanding could not be more striking. Synthesizing new forms of melanin in fibrils may well help to reveal more about its interactive properties and eventually its functional structure. Likewise, there is potential for new smart materials based on eumelanin that make use of some of its combined properties such as broad-band optical absorption spectrum, photo and electrical conductivity, anti-oxidant, paramagnetism, free radical scavenging, and ion-exchange.[10]

Acknowledgments

The authors acknowledge the support of an EPSRC/SFC Science and Innovation Award in molecular nanometrology, including a research studentship held by RMc. The assistance of Dr Paul Edwards in SEM measurements is gratefully acknowledged.

References

1. G. W. Zajac et al., "The fundamental unit of synthetic melanin: a verification by tunnelling microscopy of X-ray scattering results," *Biochim. et Biophys. Acta.* **1199**(3), 271–278 (1994).
2. C. M. R. Clancy and J. D. Simon, "Ultrastructural organization of eumelanin from sepia officinalis measured by atomic force microscopy," *Biochem.* **40**(44), 13353–13360 (2001).
3. Y. Liu and J. D. Simon, "The effect of preparation procedures on the morphology of melanin from the Ink Sac of Sepia officinalis," *Pigm. Cell Res.* **16**(1), 72–80 (2003).
4. S. Chimon et al., "Evidence of fibril-like β-sheet strcutures in a neurotoxic amyloid intermediate of Alzheimer's β-amyloid," *Nat. Struct. Mol. Biol.* **14**(12), 1157–1164 (2007).
5. E. Scherzinger et al., "Huntingtin-encoded polyglutamine expansions form amyloid-like protein aggregates in vitro and in vivo," *Cell* **90**(3), 549–558 (1997).

6. K. A. Conway, J. D. Harper, and P. T. Lansbury, "Accelerated in vitro fibril formation by a mutant alpha-synuclein linked to early-onset Parkinson disease," *Nat. Med.* **4**(11), 1318–1320 (1998).
7. M. Jastrzebska et al., "AFM investigations of self-assembled DOPA-melanin nano-aggregates," *J. Mater. Sci.* **45**(19), 5302–5308 (2010).
8. T. B. Fitzpatrick et al., "Biochemistry and physiology of melanin pigmentation" in *Biochemistry and Physiology of the Skin*, L. A. Goldsmith, Ed., pp. 687–712, Oxford University Press, New York (1983).
9. O. J. Rolinski, M. Amaro, and D. J. S. Birch, "Early detection of amyloid aggregation using intrinsic fluorescence," *Biosens. Bioelectron.* **25**(10), 2249–2252 (2010).
10. P. Meredith and T. Sarna, "The physical and chemical properties of eumelanin," *Pigm. Cell Res.* **19**(6), 572–594 (2006).
11. C. D. McGuiness et al., "Selective excitation of tryptophan fluorescence decay in proteins using a sub-nanosecond 295 nm light-emitting diode and time-correlated single-photon counting," *Appl. Phys. Lett.* **86**(26), 261911–261913 (2005).
12. G. M. Robinson and M. R. Smyth, "Simultaneous determination of products and intermediates of L-DOPA oxidation using capilliary electrophoresis with diode-array detection," *Analyst* **122**(8), 797–802 (1997).
13. S. P. Nighswander-Rempel et al., "A quantum yield map for synthetic eumelanin," *J. Chem. Phys.* **123**(19), 194901–194907 (2005).
14. K. Teuchner et al., "Femtosecond two-photon excited fluorescence of melanin," *Photochem. Photobiol.* **70**(2), 146–151 (1999).
15. D. J. S. Birch, A. Ganesan, and J. Karolin, "Metabolic sensing using fluorescence," *Synth. Met.* **155**(2), 410–413 (2005).
16. S. Meng and E. Kaxiras, "Mechanisms for ultrafast nonradiative relaxation in electronically excited eumelanin constituents," *Biophys. J.* **95**(9), 4396–4402 (2008).
17. D. M. Walsh et al., "Amyloid β-protein fibrillogenesis," *J. Biol. Chem.* **274**(36), 25945–25952 (1999).
18. T. Shirahama and A. S. Cohen, "High-resolution electron microscopic analysis of the amyloid fibril," *J. Cell Biol.* **33**(3), 679–708 (1967).
19. C. B. Andersen et al., "Branching in amyloid fibril growth," *Biophys. J.* **96**(4), 1529–1536 (2009).
20. H. C. Eisenman and A. Casadevall, "Synthesis and assembly of fungal melanin," *Appl. Micro. Biotechnol.* **93**(3), 931–940 (2012).
21. G. Zonis et al., "Melanin absorption spectroscopy: a new method for noninvasive skin investigation and melanoma detection," *J. Biomed. Opt.* **13**(1), 014017 (2008).
22. K. Kashihara, T. Shinya, and F. Higaki, "Neuromelanin magnetic resonance imaging of nigral volume loss in patients with Parkinson's disease," *J. Clin. Neurosci.* **18**(8), 1093–1096 (2011).
23. T. Pan, X. Li, and J. Jankovic, "The association between Parkinson's disease and melanoma," *Int. J. Cancer* **128**(10), 2251–2260 (2011).